RANDOM ACCESS RENDERING OF ANIMATED VECTOR GRAPHICS USING GPU

I. LEBEN

Supervisor: G. LEACH

Honours Thesis

School of Computer Science and Information Technology
RMIT University
Melbourne, AUSTRALIA

October, 2010

Abstract

Efficient random access to image data allows texture mapping of images onto curved surfaces to be accelerated by the GPU. This property has traditionally been associated with raster images, while a typical vector image representation cannot be directly interpreted by the established GPU architecture. In order to be accelerated, the vector image data needs to be first changed into a suitable representation. Recent research allowed texture mapping of vector images by taking advantage of the programmable stages of the GPU. However, the new rendering approach introduces an expensive preprocessing step running on the CPU. In this thesis we investigate the techniques to fully accelerate vector image rendering and texture mapping on the GPU, including the preprocessing steps. We present an alternative localised vector image representation and an efficient parallel preprocessing algorithm, suitable to implementation and acceleration on the GPU. Our approach makes use of the recent advances in the GPU architecture to facilitate and improve the gains from parallelism in the encoding algorithm. We analyse the memory requirements and performance of our GPU implementation and compare it to a sequential CPU implementation and the use of traditional raster images.

Contents

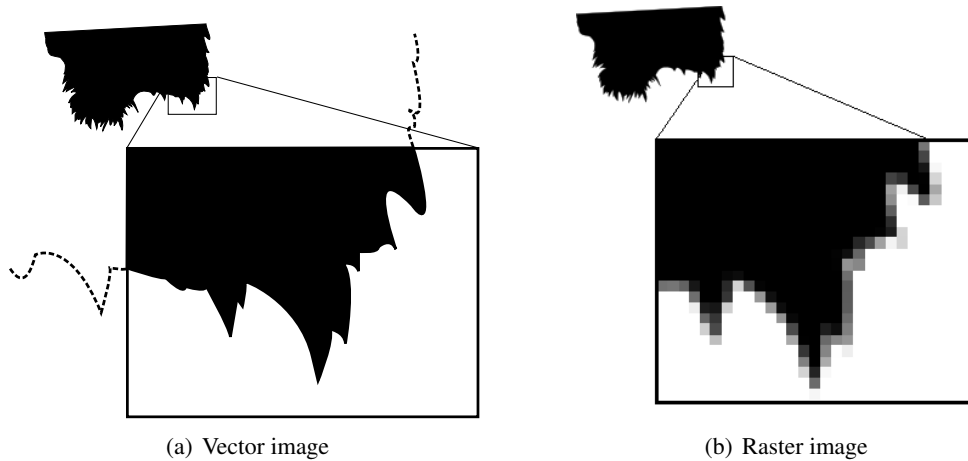(a) Vector image   (b) Raster image

Figure 1: Vector images retain sharp colour discontinuities even at large zoom, while raster images suffer from noticeable artifacts.

1   Introduction

Random access rendering is a method whereby the colour of an image is computed at an arbitrary image space coordinate in an arbitrary order. Efficient random access to image data is a requirement for texture mapping and has traditionally been associated with raster images. The definition of a raster image as a grid of coloured pixels lends itself perfectly to the random access scheme. However, the main drawback is the artifacts such as jagged or blurred edges arising from missing detail in information when the image is scaled.

In contrast, vector graphics use mathematical equations and shapes to describe coloured regions. Such a definition allows scaling of a vector image while retaining sharp edges at colour discontinuities. As illustrated in Figure 2, in order to classify a point as inside or outside a vector shape, we need to consider all of its primitives. Moreover, when rendering a small portion of a shape under large zoom, the parts outside of the visible area still need to be processed, adding to unnecessary overhead as the zoom factor increases. This makes straightforward approaches to random access inefficient and has until recently prevented the use of vector images as textures.

Applications of vector graphics are many, ranging from high detail maps to general scalable user interfaces. An efficient random access algorithm would further broaden the usability of vector images. Regions of a map outside of the view could be efficiently discarded as the user zooms in on a particular detail. Graphical user interfaces could be mapped onto surfaces in 3D space allowing new ways of navigation and better screen estate management.

Historically, Graphics Processing Units (GPUs) have specialised into rendering of triangle primitives and have no built-in support for rasterization of curved shapes present in vector images. Nonetheless, dependency on the triangle-based rasterization has been alleviated by the increase in GPU programmability. Recently, [NH08] have developed a rendering technique that evaluates vector shapes directly in the programmable stages of the GPU, after localising the vector data in an expensive preprocessing step on the CPU. This allows efficient random access, but limits the use to static non-animated graphics.

An important thing to consider is the paradigm shift taken by an approach such as [NH08]. The traditional graphics pipeline starts with triangle and line primitives and rasterizes them into the framebuffer. Where primitives overlap, this results in multiple executions of the same processing instruc-
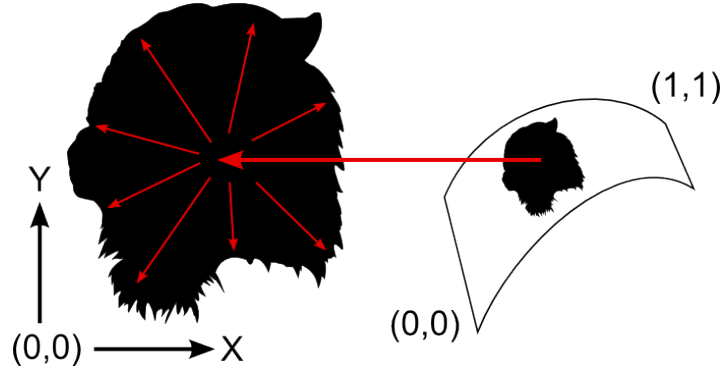
Figure 2: Straightforward approaches to random-access rendering of vector images are inefficient. To find the colour of one textured pixel on the screen, all the segments of the shape need to be processed.

tions for a single pixel with regard to a different primitive. In contrast, the approach being discussed preprocesses the entire set of primitives in the scene to build a look-up data structure. In the final rendering stage, all the primitives affecting a given pixel can be looked up efficiently in a single execution of processing instructions to determine the colour of the pixel. It is important to note that such an approach increases the per-pixel processing complexity, but is facilitated by the recent advance in graphics hardware architecture.

The focus of this research is to extend the above approach by investigating alternative vector image data structures and preprocessing techniques, suitable to parallelisation and acceleration via the GPU. Our goal is to implement the entire rendering process, including the preprocessing steps, on the GPU. By taking advantage of the parallel architecture, great improvement in performance is achieved, allowing application to animated vector images where continuous preprocessing is required.

In general, this thesis investigates the following questions:

1. How to efficiently accelerate vector image localisation using the parallel architecture of the GPU?

2. Is there an alternative localised vector image representation, more suitable to parallel encoding and rendering?

3. What are the performance gains of a parallel preprocessing algorithm compared to a sequential CPU implementation?

4. What degree of vector data localisation provides an optimal balance between preprocessing and rendering time?

5. What is the benefit of vector data localisation with regard to animated vector graphics where continuous preprocessing is required?

2 Background

2.1 Vector Image Definition

A vector image is a set of vector shapes, each defined as an open or closed spline of straight line and curved segments. Closed shapes can be filled, meaning the spline defines a border between the
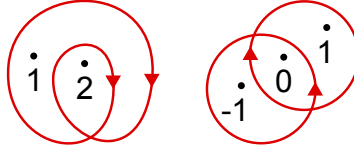
Figure 3: Points in curves and their respective winding numbers.
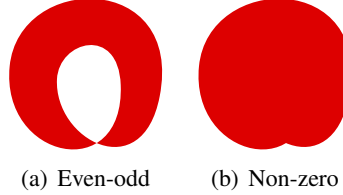

(a) Even-odd   (b) Non-zero

Figure 4: Same shape filled using two different fill rules.

exterior and the coloured interior of the shape. Shapes can also be stroked, meaning the boundary has a visible thickness. For practical purposes, stroked shapes can be adequately approximated by another more complex vector shape describing the resulting outline of the thick line, thus reducing the definition to closed, filled shapes.

The interior of the filled shapes is determined according to the value called *winding number*. For any point, the winding number represents the total number of times that the curve travels around the point. Clockwise movement counts as positive whereas anticlockwise movement counts as negative. Figure 3 shows examples of points in curves and their respective winding numbers. Note that one shape can consist of multiple contours in which case the winding number is the sum of the individual winding numbers of all the contours.

There are two common rules for determining the interior of a shape based on the winding number, namely *even-odd* and *non-zero*. The former classifies the areas with an odd winding number as interior while the latter considers any area with a winding number different than 0 to be inside as shown in figure 4.

2.2   Evaluation of Spline Segments

Individual segments of a vector spline are most commonly defined using Bézier curves of first to third degree, as described in [Far02]. In general a Bézier curve of degree n is defined as follows:

$$\mathbf{B}(t) = \sum_{i=0}^{n} \mathbf{b}_{i,n}(t)\mathbf{P}_i, \quad t \in [0,1]$$

where the points $\mathbf{P}_i$ are called *control points* of the Bézier curve and the polynomials

$$\mathbf{b}_{i,n}(t) = \binom{n}{i} t^i (1-t)^{n-i}, \quad i = 0,...n$$

are known as Bernstein basis polynomials of degree n with the following property:

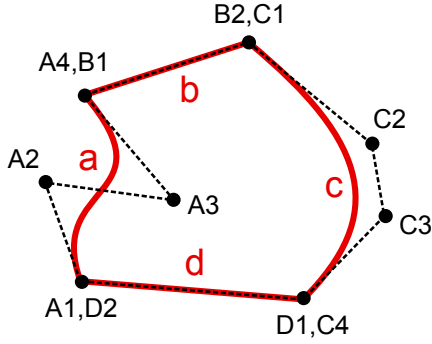$$\sum_{i=0}^{n} \mathbf{b}_{i,n}(t) = 1, \quad t \in [0,1]$$

Figure 5: A closed spline (red) consisting of two line segments and two cubic Bézier curve segments with its control polygon (black).
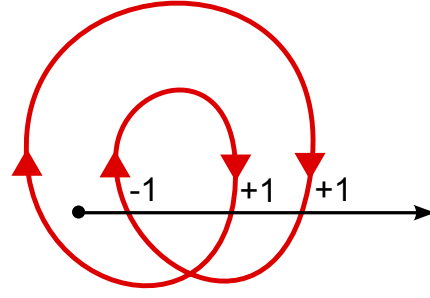
Figure 6: The direction of the intersections between a horizontal ray and the segments of a spline count towards the winding number of the point.

meaning that the sum of all the polynomials of the same degree is always 1. The Bézier curve equation therefore interpolates between the given control points according to the parameter t, beginning exactly at $\mathbf{P}_0$ and ending exactly at $\mathbf{P}_n$. A curve of degree n has $n + 1$ control points. A Bézier curve of degree 1 is essentially a straight line. Consecutive spline segments share a control point where one ends and the next one begins. The ordered set of control points of all the segments defines the *control polygon* of the spline as shown in figure 5.

A simple way of finding a point on the Bézier curve at an arbitrary parameter value is to substitute the value into every basis function, compute the products with the respective control points and add them together. While straightforward, this approach is not numerically stable. Instead, as described in [BM99] we can evaluate the points on the curve by recursive subdivision of the sides of its control polygon. This technique, known as *de Casteljau's algorithm* reduces numerical errors during the course of evaluation.

2.3 Winding Number Evaluation

The Bézier curve equations can also be used to evaluate the winding number of any point with regards to a vector spline. We start by casting a ray from the point in an arbitrary direction. Based on the *Jordan Curve Theorem*, the point is found to be inside the polygon, if the ray crosses an edge of the polygon an odd number of times. Counting the number of intersections gives a value known as the *crossing number*. Now, by checking the direction of the intersecting edge, we instead add $+1$ for every left-to-right crossing and -1 for every right-to-left crossing. The resulting value is the winding number of the point.

Imagine the ray is being cast from point $P(x, y)$ horizontally in the positive direction of the x axis. We can find an intersection with any segment of the spline by finding the roots t_i of the equation $y = y(t)$ where $y(t)$ is the linear or higher order polynomial describing the spline segment. When $t \in [0, 1]$ and $x < x(t)$, the ray intersects the segment.

Obviously, the winding number at any point depends on the geometry of the entire shape outline. It is this requirement that poses the greatest obstacle when designing an efficient random access rendering algorithm.
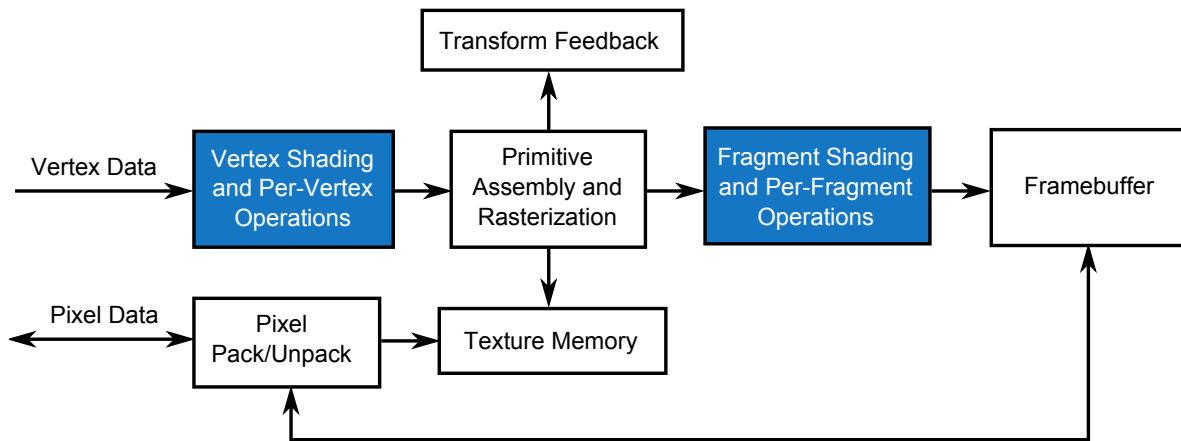
Figure 7: OpenGL rendering pipeline. Programmable parts are coloured in blue.

2.4   Traditional Graphics Pipeline

Traditional display devices require input in the form of a grid of colour values, called a *raster*. A colour value in a raster is called a *pixel*. For a graphical object to be displayed, the pixels covered by its shape need to be determined in a process called *rasterisation* and the colour values in the display raster changed accordingly. The architecture of modern GPUs is optimised for rasterisation of three types of primitives: points, lines and triangles. The roots of this design reach into the early history of computer graphics when parallel computing architecture was not as powerful and programmable as today. Triangle rasterisation coupled with texture mapping of raster images was much simpler to implement in hardware compared to direct evaluation of higher order mathematical equations. Thus more complex shapes have to be converted into the basic primitives by tesselation, in order to accommodate and benefit from hardware-accelerated rendering.

The GPU has evolved enormously in terms of speed and programmability, however the fundamental approach has not changed much, with the triangle rasterisation unit remaining a core built-in component. Nonetheless, the increase in programmability has enabled new ways of using the GPU.

Firstly, programmers can now write code that defines the behaviour of certain stages of the rendering pipeline as exposed by the graphics APIs such as OpenGL and DirectX. The pipeline is still based around points, lines and triangles being the basic rasterisable primitives, however, custom programs for processing of vertices and pixels can be uploaded onto the hardware. The stage processing the vertices is called a *vertex shader*, while the pixel processing stage is named a *fragment shader*.

More importantly, new programming interfaces have emerged that expose the GPU hardware as a general-purpose multi-core computing device. APIs such as CUDA and OpenCL allow programmers to supply data and upload the code onto the GPU to process that data by hundreds of processors in parallel. This approach, known as *GPU Computing*, may be completely devoid of any graphics-related paradigms, although often the results of computation are used for graphical purposes or end up being visualised via traditional rendering pipeline.

2.5   Recent Advances in GPU Architecture

new programmable stages
    fast memory cache
    atomic operations

memory writes to arbitrary location

3   Previous Work

In a typical CPU implementation of a vector graphics renderer, every spline is first approximated by linear segments. Intermediate points on the curved segments can be obtained in a straightforward manner by curve evaluation at a fixed step. Alternatively, the process can be optimised via adaptive algorithms which generate less points in the straight regions and more points in the regions of higher curvature. Common approaches include forward difference evaluation and recursive subdivision based on de Casteljau algorithm. The interior of the resulting piecewise linear polygon is triangulated according to the fill-rule applied to the shape. Finally, the triangles are rasterized into the framebuffer.

Unfortunately, the known curve subdivision and polygon triangulation algorithms are expensive in terms of required processing time compared to the final rendering of the image. Moreover, they are inherently sequential, which means they cannot be efficiently parallelised and therefore cannot take advantage of the GPU.

3.1   Forward rendering approaches

[LB05] have developed an approach where the implicit equation of quadratic curves is evaluated directly in the fragment shader to perform inside/outside classification. They start by observing that "the implicit form of any rational parametric quadratic curve is a conic section; and that any conic section is the projected image of a single canonical parabola." They show that a quadratic curve with control points $(0, 0)$, $(0.5, 0)$, and $(1, 1)$ plots the quadratic curve $v = u^2$ exactly. They assign these points as the (u, v) texture coordinates to the vertices of a triangle. Suppose the vertices are the control points of another arbitrary quadratic curve. As the hardware interpolates the texture coordinates across the triangle, it essentially projects the quadratic curve from texture space into screen space. They determine if the pixel is inside or outside the curve by evaluating $f(u, v) = u^2 - v$ in a pixel shader program. If $f(u, v) < 0$ then the pixel is inside the curve, otherwise it is outside.

This removes the need for curve subdivision, but the interior of the shape still needs to be triangulated. [KSST06] combine the projective rendering of the quadratic curves with a stencil polygon rendering technique. First, an arbitrary pivot point is selected. For each linear segment a triangle is drawn with one of its vertices at the pivot point and the other two at the vertices of the line segment. For each quadratic segment a triangle is drawn between the pivot point and the first and the last control point, skipping the middle control point. Additionally, a triangle is drawn for each quadratic curve, discarding the pixels based on the projective technique of [LB05]. For every pixel drawn, the binary value in the stencil buffer is inverted. After all the triangles have been drawn, the values in the stencil buffer essentially represent the crossing number for every point as if the intersection ray was cast towards the pivot point. This allows the pixels in the framebuffer to be coloured according to even-odd fill rule.

3.2   Random access rendering by image localisation

The algorithms described so far enable efficient rendering of animated vector graphics. However, they are based on forward oriented triangle rasterisation. Instead, we are aiming for a random-access scheme, where the pixel colours might be queried simultaneously by multiple fragment shaders at an

arbitrary point within the vector shape in an arbitrary order. To achieve this, we need to be able to evaluate the winding number of any point in the image space from within the fragment shader.

[NH08] presented an approach to this problem that localises the vector image representation to coarse lattice cells in a preprocessing step. Each cell contains a localised description of the graphics primitives it overlaps. This information is encoded into a texture and interpreted by the fragment shader. For every fragment, the vector data is read from the lattice cell that the texture coordinate falls in. The winding number is calculated using the ray-casting intersection technique, but thanks to the localisation, only the segments overlapping the cell need to be considered. They observe that increasing the lattice resolution decreases the number of spline segments to intersect per pixel, as long as the detail in the image is fairly uniform. This in turn reduces the rendering time and increases the achievable rendering framerate. However, they find that the preprocessing takes too long for real-time use which prevents their approach to be used with animated images.

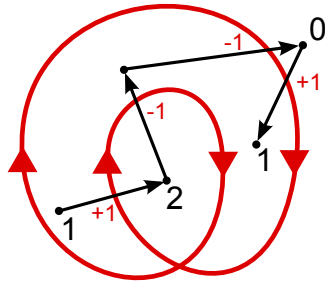## 4   Pivot-Point Localised Image Representation

Figure 8: Starting from a known winding number, the winding number of adjacent regions can be determined by a single crossing of an edge.
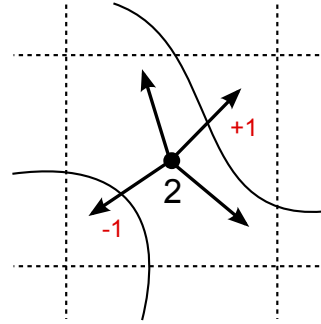
Figure 9: Casting a ray from the pivot point and intersecting the segments in the cell gives the winding number of any other point within the same cell.

In order to take full advantage of the parallel architecture of the GPU, it is first necessary to find a suitable localised image representation satisfying two conditions. On the one hand, the representation must exhibit a high degree of localisation to allow efficient random-access. On the other hand, this representation must be obtainable via some process which can achieve a high degree of parallelism.

Like [NH08], we create a coarse lattice across the original vector image. However, our approach differs in the contents of the lattice cells. To preserve the winding number within a cell, their algorithm creates auxiliary segments on the right boundary of each cell. The direction of the auxiliary segments affects the resulting winding number and depends on the segments in other cells, to the right of the cell in question. Therefore, for every segment crossing a cell, the winding number needs to be integrated into the cells to its left. The dependency of each cell on the contents of other cells makes it challenging to devise a parallel localisation algorithm.

Instead, we start by observing that the winding number of any region in a vector shape can be determined by a single crossing of an edge, as long as the winding number of another adjacent region is known. As shown in figure 8 it is possible to move from one region to another, adjusting the winding number according to the direction of the crossing edge and thus finding the winding number of every region. We take advantage of this observation by assigning a *pivot point* to every cell and finding the

winding number of that point in the preprocessing step. The location of the pivot point is implicitly defined at the centre of the cell. While [NH08] cast a horizontal ray in the positive x direction, we cast a ray from the pivot point of the cell in an arbitrary direction, towards any other point in the cell. The intersections of the ray with vector segments crossing the cell give the change in winding number from the original winding number of the pivot point.

Our localised image representation thus consists of a set of lattice cells containing a pivot winding number and the intersecting spline segments. No additional auxiliary segments are required. We will now describe the process of obtaining the winding numbers of the pivot points. Imagine each cell being a pixel of a low-resolution image. The winding number parity at the pivot point can be obtained by sampling the vector image at the centre of the pixel. Now, we have already described a technique of forward rendering of vector images presented by [KSST06]. Therefore, to obtain the grid of winding numbers we essentially render the image using the forward rendering technique at a low resolution matching the size of the pixels to the size of the lattice cells. When an even-odd fill rule is in use, the inversion operations on the stencil buffer used by [KSST06] give the required winding number parity. In the case of non-zero fill rule, the stencil operations are modified to produce the actual winding number.

Our final rendering algorithm combines the grid of winding numbers with the vector segment data encoded into variable-length cell streams described by [NH08]. Each cell stream encodes the control points of the segments crossing the respective cell, so the encoding process involves intersection of vector segments with the lattice cells. The work done so far implements the creation of winding grid on the GPU, while the cell stream encoding is done on the CPU. The future efforts of this research will investigate the implementation of cell stream encoding using the GPU.

5 Encoding

In order to be able to compare the performance of the two approaches, we implemented the encoding pass and the rendering pass on the GPU for both our pivot-point representation as well as the auxiliary-segment representation used by [NH08].

5.1 Memory interface

The input to the encoding algorithms is given in the form of vertex buffers uploaded onto the GPU. The output is also stored in the GPU memory and directly reused by the rendering stage. Since the entire process of encoding and drawing is repeated in every frame, the output buffers can be reused between multiple images. This means the upper bound on the memory used by our approach is equal to the memory requirements of the largest image ever being drawn and does not increase when additional vector images are used in the same scene.

Our GPU implementation of the image encoding would not be possible without read and write access to an arbitrary location in the GPU memory. We have considered both the EXT_shader_image_load_store and the NV_shader_buffer_store extensions for the output buffers and memory access interface. The convenience offered by the EXT_shader_image_load_store is the explicit dimensionality in the memory access. This could be advantageous in the parts of the algorithm dealing with a 2-dimensional grid. However, due to the limited maximum size of a dimension of an OpenGL texture, this same property of the interface proved to be an important setback in the parts of our algorithm that require a long one-dimensional array. For this reason, we chose to use the NV_shader_buffer_store which did not limit us in any way with regard to the size of the accessible memory in any dimension. Blocks of

memory which represent a 2-dimensional grid are mapped onto a one-dimensional array in row-major order.

A convenient advantage of the NV_shader_buffer_store is the ability to cast the memory pointer to a different type and thus view parts of the same block of memory as a different data type. This allows the memory to be viewed through C-like structures defined in the shader code and thus store integer and floating point numbers of different bit sizes next to each other. Unfortunately, our time constraints did not allow us to investigate the potential advantages of such an approach. Instead, we allocate all the GPU buffers as a 32-bit integer or floating point array and always use them through the pointer of the same respective type. It might also be worth investigating the performance and memory advantages of using 16-bit precision variables in various parts of our data structures. This was left for future work.

5.2   Algorithm input

Our implementation requires minimal setup by the CPU which includes the following steps:

1. Approximate cubic curve segments with multiple quadratic segments.

2. Compute the coarse bounding box of the entire image and every separate object based on the segment control points.

3. Compute the memory size of the main grid and object sub-grids to format the grid memory pool.

4. Upload the object grid offset indices and segment control points into the GPU buffers.

We designed the input structures so as to minimize the data required to be sent to the GPU on every frame. The input required by every rendering pass of our encoding algorithm is represented with the least amount of data that defines the respective geometry. Objects are represented by a line primitive extending from the minimum point to the maximum point of the object's bounding box. Straight line segments are represented directly by a line primitive. Quadratic curve segments are represented by a triangle which encodes the three control points of the curve.

5.3   Data structures

Both encoding algorithms use the same input and output data structures. The only difference is in the minor additional data generated by each representation respectively. The exact differences are described in the subsequent sections.

Figure 10 shows the three intermediate buffers used. The synchronisation buffer and the grid buffer are allocated as a 32-bit integer array. They hold counter variables which are accessed during the algorithm via atomic operations to synchronize encoding of the interleaved cell streams. The synchronisation buffer holds just a single global stream length counter. The grid buffer holds several counters for every cell of the main grid as well the smaller object grids. The purpose of each of the grid counters is described later in the algorithm details. The object grids hold their own set of these same counters which are required to be able to process segments of multiple objects simultaneously and thus maximise the achievable level of parallelism. The size of an object grid is determined by the bounding box of the respective object. However, the cells of these sub-grids are aligned with the cells of the main grid, so that the information can be assimilated and propagated to the main grid at the end of the encoding.

Sync Buffer

Grid Buffer

Stream Buffer

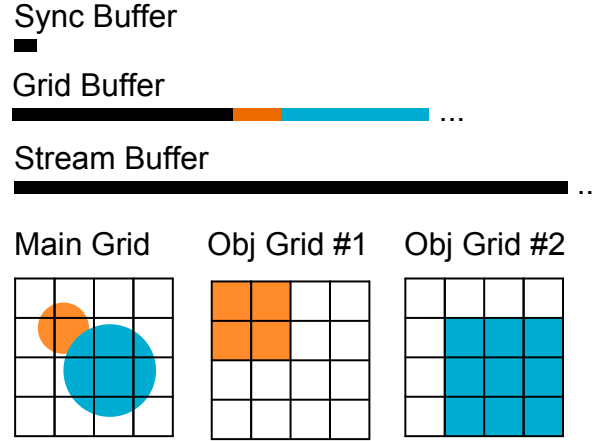Main Grid   Obj Grid #1   Obj Grid #2

Figure 10: Three buffers used by the encoding algorithm. The main indirection grid and the stream buffer are the input to the rendering pass.

The stream buffer is allocated as a 32-bit floating point array. It holds the cell stream data represented as interleaved linked lists. Each cell stream belongs to one cell in the main grid and encodes the spline segments or auxiliary segments intersecting that cell. Each node of a linked list encodes the control points of a spline segment or an object info header.

5.4 Linked list cell streams

The data in the stream buffer is organized into nodes of different types, inter-linked via the stream index of the first data in the node. Different nodes have different number of data values and therefore different sizes. The first value in every node defines the type of the node. The second value in every node is the link to the previous node in the same list. The following values in the node encode the control points of the line or quadratic curve segment or the properties of an object.

Such organisation allows us to interleave multiple lists within the same memory space. One list contains segments of one particular object intersecting one particular grid cell. There might be multiple objects intersecting the same cell, which results in multiple linked lists per cell. The counters in the object sub-grids are used to facilitate concurrent construction of lists for all the object within the same cell as described below.

The variables used in the list construction are the following:

1. Atomic counter L in the synchronisation buffer holding total stream length

2. Atomic counter H in a cell of the grid buffer holding stream index of the first node (list head)

3. Size S of the new node as number of stream words

4. Stream index I of the new node in the list

5. Stream index P of the previous node in the list

The node insertion algorithm is as follows:

```
I = atomicAdd( L, S )
P = atomicSwap( H, I )
```
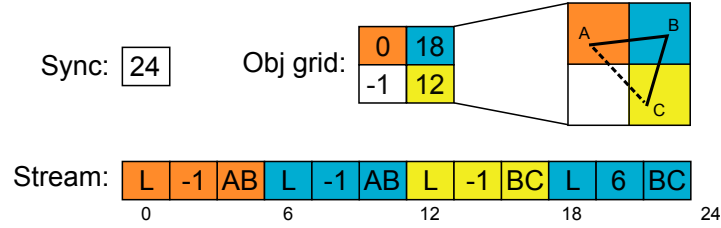
Figure 11: The state of the stream buffer and synchronisation counters after the first two segments of a triangle shape are processed.
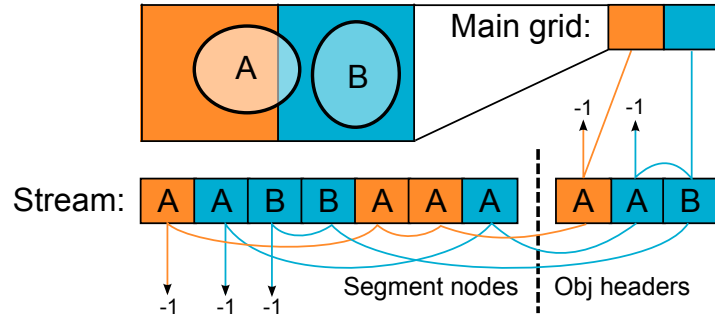

Figure 12: The stream buffer contains interleaved nodes of multiple linked lists. Each linked list contains segments of one particular object intersecting one particular grid cell.

```
stream[ I ] = nodeType
stream[ I+1 ] = P
stream[ I+...] = additional node data...
```

where *atomicAdd* function adds the given value to an atomic counter and *atomicSwap* function swaps the value of the atomic counter with the new value. Both atomic functions return the old value read prior to the modification.

The segment encoding pass uses atomic counter H in the sub-grid of the object to which the current segment belongs. By using separate head pointers for every object, multiple linked lists per cell can be constructed concurrently, which are then assembled in another pass encoding the object info headers. The object encoding pass uses the atomic counter H in the main grid, but reads the H counter from respective object grid cell and stores it into the object header node. This results in a single linked list per cell of the main grid containing object headers, where each object header points to another linked list containing the object segments intersecting the cell. Figure 12 illustrates one possible final structure of a stream buffer.

The final back-to-front sorting pass iterates through the object header linked list for every cell and sorts the contents of the nodes based on the index of the object in the vector image.

5.5   Parallelism

Parallelism in our implementation is achieved by distributing the processing of geometry between multiple shader processors on the GPU with regard to segments, control points or grid cells.

The first level of parallelism is achieved with the vertex shaders, where multiple control points are processed simultaneously. The second level of parallelism is achieved with the geometry shaders, where additional processing such as bounding box computation can be applied to multiple segments

simultaneously. The third and final level of parallelism is achieved with the fragment shaders, where processing can be applied to multiple grid cells simultaneously.

This is the coarse description of our encoding algorithm in pseudocode, excluding the details that differ between the auxiliary-segment and pivot-point representations:

```
init stream length counter to 0

for (every main grid cell)
   init main cell counters to -1
loop

for (every object)
   for (every object grid cell in bbox)
      init object cell counters -1
   loop
loop

Init object grid counters

[Sync memory]

for (every object)
   for (every line segment)
      find line bounding box
      for (every object grid cell in bbox)
         if (intersects cell)
            encode segment into cell stream
         loop
      loop
   loop
   for (every quadratic segment)
      find quad bounding box
      for (every object grid cell in bbox)
         if (intersects cell)
            encode segment into cell stream
         loop
      loop
   loop
loop

[Sync memory]

for (every object)
   for (every object grid cell in bbox)
      encode object header into cell stream
      link main grid cell to the object header
```

```
   loop
loop

[Sync memory]

for (every main grid cell)
   sort object headers in the stream back-to-front
loop

[Sync memory]
```

Note that due to the previously described parallelisms the steps of every loop actually run simultaneously. Each top-level for loop is a separate rendering pass. The passes of the form

```
for (every main grid cell)
```

are implemented as drawing of a rectangle over the entire main grid. The transformation matrices are set so as to match the size of a covered pixel to the size of one grid cell. This gives us MxN invocations of the fragment shader, where MxN is the size of the main grid. Per-cell processing is implemented in the fragment shader so that each invocation of the shader computes the results for its respective cell. The passes of the form

```
for (every line\quad segment)
   for (every object grid cell in bbox)
   loop
loop
```

start off as drawing of a line or triangle primitive. The geometry shader takes in two or three control points defining the segment and computes their bounding box by combining their minimum and maximum coordinates in each dimension. The minimum coordinates are rounded down and the maximum coordinates are rounded up to the nearest grid cell. The geometry shader then discards the line or triangle primitive and emits a rectangle covering the cells within the bounding box. Again, this results in an invocation of a fragment shader for every cell that is potentially intersected by the line or quadratic segment. The passes of the form

```
for (every object)
   for (every object grid cell in bbox)
   loop
loop
```

are initiated as drawing of line segments extending from the minimum to the maximum point of the object bounding box rounded to the nearest grid cell. These coordinates are precomputed in the setup stage, since they are required to format the grid memory pool. Same as in the other two cases above, the geometry shader simply discards the line segments and emits a rectangle matching the bounding box instead.

We described previously, how separate blocks of memory cache are being used on every cache level for each group of shading processors. The concurrency in access to memory might result in memory discrepancies as seen by two processors belonging to a different group. It is important to note that none of the points of memory synchronisation are inside a loop, which means the number of required synchronisations is fixed and does not increase with the complexity of the input data.

This was especially challenging to achieve on the level of objects when an image consists of more than one shape of different colors. The linked lists of segments for each object need to be separated, so that the inside/outside classification can be done on per-object basis within each cell. As described in detail later, this required additional object sub-grids that hold object-specific synchronisation counters, so that separate segment linked lists could be maintained for every object that intersects a grid cell.

The following two sections describe in detail the differences in the encoding algorithm between the two target localisation representations.

5.6 Auxiliary-segment localisation

Our auxiliary-segment localisation algorithm is a GPU implementation of the "fast lattice-clipping algorithm" used by [NH08] with minor adjustments in order to improve the parallelism. The line segment and quadratic segment encoding passes of our algorithm perform the cell boundary intersection tests and compute the change Δh in winding number. The object header encoding pass performs insertion of auxiliary vertical segments based on the final winding number sum h.

We use the same boundary conditions to insert auxiliary vertical segments on the right edges of the cells. However, rather than assimilating the running sum of Δh in the object encoding pass, we update the sum across all the cells in the same row to the left of the current cell as soon as an intersection with a segment is found in the segment encoding pass. Although more work is done in total this way, our approach proved to work better in parallel, achieving a noticeable speed-up.

The reason for this is that the complexity of the segment encoding pass is much higher than the complexity of the final object header encoding pass. Since the Δh is read and written concurrently from multiple shaders, it needs to be accessed through atomic operations. The result of every atomic operation needs to be synchronised between the local caches of multiple shading processor groups. Due to the higher complexity, there is more time between invocations of the segment encoding shader to perform the synchronisation, before the result needs to be read by another invocation, so the impact on the performance of the entire rendering pass is much lower.

When the object header encoding pass begins, the grid cell counters already contain the final winding number sum h, which can then be used directly, to insert additional auxiliary segments, before the linked list is closed with an object header.

5.7 Pivot-point localisation

In our pivot-point localisation algorithm the segment encoding pass computes the exact winding number with regard to the entire object shape for the pivot point of every object grid cell. To this end, the segment encoding shader needs to compute not only the intersection between the segment and the cell, but also the intersection between the segment and the horizontal rays cast from the pivot points of every cell to the left.

To parallelise the computation of the ray-segment intersections, we extend the segment bounding box rectangle on the left side all the way to the left edge of the respective object grid. This gives us additional shader invocations for the grid cells to the left of the segment.

Each fragment shader invocation computes the ray-segment intersection for the respective pivot point and updates the winding number counter in the object grid cell with an atomic operation. When the object header encoding pass begins, the grid cell counters contain the final winding number of their pivot point. This winding number is stored into the object header and used in the rendering pass to offset the winding number obtained with segment intersections between the pivot point and an arbitrary point inside the cell.

6 Rendering

6.1 Antialiasing

7   Results and Analysis

In order to evaluate and compare the implemented approaches, we measured their required memory size, encoding and rendering performance, as well as combined performance of the two stages, which comes in effect when rendering animated images.

All results were obtained using Intel Core i7 2.80 GHz CPU and NVIDIA GTX460 1GB GPU. Two different images were used in our tests: the tiger image, which has long been the traditional subject of benchmarking, as well as a block of text containing variable numbers of glyphs.
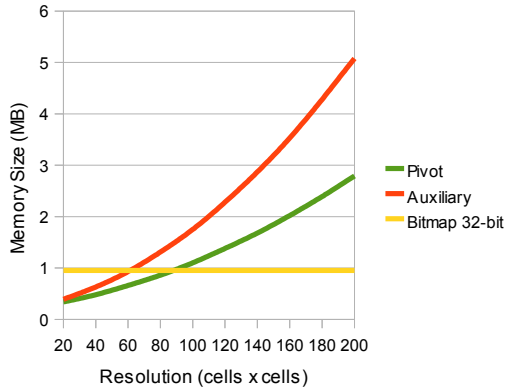
Figure 13: Total memory size of the stream data as a function of lattice resolution for the tiger image in Figure 19.
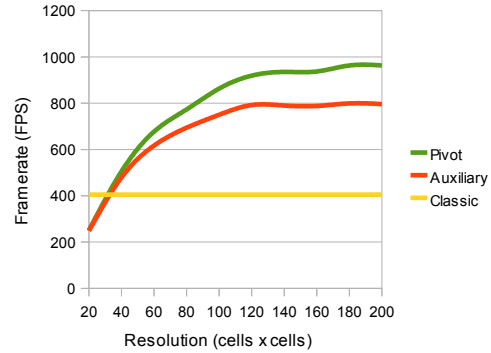
Figure 14: Rendering speed as a function of lattice resolution for the tiger image in Figure 19.

7.1   Memory Requirements

Figure 13 shows the total memory size of all the cell stream data, at various lattice resolutions. This is the effective size of the encoded vector image residing in the GPU memory which needs to be kept for continuous rendering.

Despite the similarity in approach, the memory requirements of our implementation are generally higher than those achieved by [NH08]. This is mainly due to two important design choices. Firstly, the straightforward approximation of cubic curves with a fixed number of four quadratic segments greatly increases the total number of segments in the encoded image. This could be much improved by implementing a more flexible adaptive approximation. Secondly, due to the parallelism in our cell stream construction, the segments might be encoded into the stream out of order, so the end and start point of two consecutive segments cannot be shared and needs to be encoded twice in the node of each segment.

Nonetheless, considering the diminished gains in rendering performance at large lattice resolutions, the memory requirements of our encoded vector image do not gravely exceed those of a traditional bitmap image. As described in the following section, the rendering performance with the same image reaches a plateau around resolution of 120x120 cells. At that grid size our pivot-point representation barely exceeds the memory size of a 32-bit bitmap image of the same pixel size at 1:1 scale, while offering all the advantages of vector image scalability.

It is also worth noting, that our pivot-point representation requires significantly less memory than the auxiliary-segment representation, especially at higher grid resolutions, since the fully opaque cells
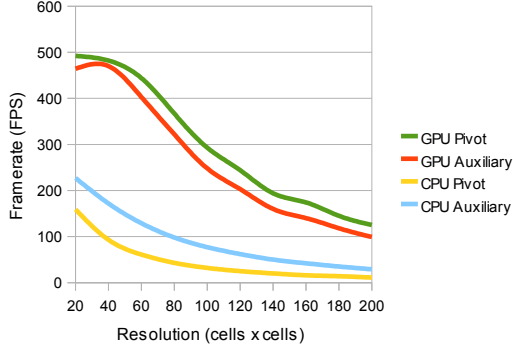
18

Figure 15: Encoding speed as a function of lattice resolution for the tiger image in Figure 19.
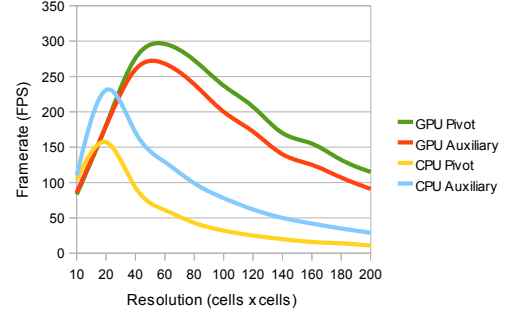
Figure 16: Encoding + rendering speed as a function of lattice resolution for the tiger image in Figure 19.

do not require an auxiliary segment to mark them as interior.

7.2 Encoding and Rendering Performance

As seen on Figure 15 our GPU implementation offers significant improvement in encoding performance over the CPU approach. Even at higher grid resolutions, when the CPU performance starts dropping below rate of 30 frames per second, the GPU encoding remains well above the interactive threshold.

It is interesting to see the GPU was faster at performing pivot-point encoding than auxiliary-segment encoding, while the opposite holds for the CPU. The CPU results can be explained by the greater simplicity of maintaining the auxiliary counter compared to the computation of ray-curve intersections at pivot points. On the other hand, that same factor doesn't seem to affect the GPU encoding, which hints at the atomic operations still being the bottleneck of the approach.

Figure 14 plots the rendering speed as a function of lattice resolution. The framerate sharply increases at lower resolutions and eventually reaches a plateau. At that point the resolution of the grid becomes high enough that further increase in resolution does not result in any significant decrease in the number of segments per cell. This point varies with the level of detail in the image, so the optimal lattice resolution depends on the image being rendered. Again, our pivot-point representation performed faster than auxiliary-segment representation, due to the lower number of segments per-cell.

We also measured the effective framerate in an animated image scenario, where both encoding and rendering have to be done on each frame. Figure 16 shows the results at various lattice resolutions. Both the CPU and the GPU data lines show a clear point at which the balance between encoding and rendering speed was optimal. This point mainly depends on the slower of the two components. In our case, faster GPU performance in encoding and rendering also results in higher optimal resolution and higher achievable combined framerate over the CPU approach.

7.3 Comparison with Traditional Forward Rendering

We compared our random access rendering technique against the traditional forward rendering as described in [KSST06] by rendering the vector image at various levels of scale. Figure 17 plots the framerate as a function of image screen size after scaling.
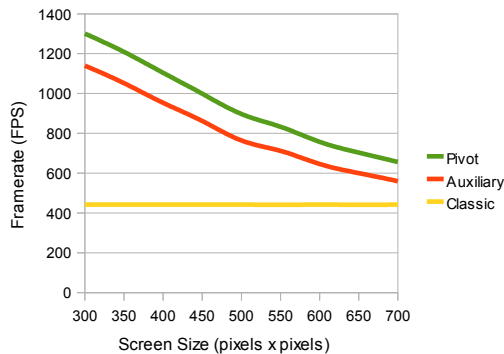
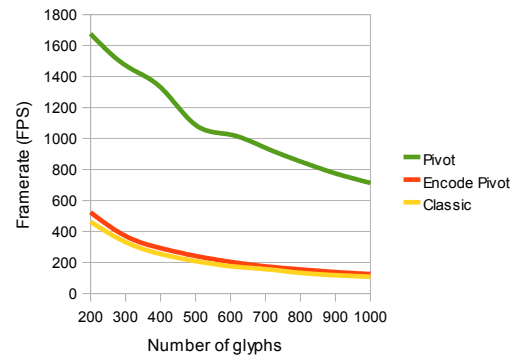Figure 17: Rendering speed as a function of actual image screen size for the tiger image in Figure 19.

Figure 18: Rendering speed as a function of number of glyphs for the text image in Figure 19.

With the forward rendering approach, the entire geometry of the image needs to be processed on every frame. For this reason, the geometric complexity is by far the most important factor affecting the framerate. In fact, the complexity of the tiger image is so high, that it governed the performance of traditional rendering entirely and there was no noticeable slowdown at larger levels of scale.

On the other hand, the random-access rendering is more alike to bitmap texturing; at large enough levels of lattice resolution, the geometric complexity is removed from the rendering stage and the number of textured pixels becomes the most significant performance factor. However, our random-access rendering performed so much faster in general, that it still achieved higher framerate than forward rendering even at larger levels of zoom. The results on Figure 17 were achieved with a grid resolution of 120x120 cells.

To see the effect of the level of geometric complexity on the two rendering techniques, we used an image containing a block of text using vector glyphs. Figure 17 shows the effective framerate as the number of letters (and therefore glyph objects) in the image increases. For random-access rendering, the lattice resolution was being adjusted dynamically, so that each letter in the text covered roughly a 2x2 block of cells. This time, the increasing geometric complexity noticeably affected the forward rendering technique. The framerate of random-access rendering was also decreasing with the number of glyphs, since a larger number of pixels was being coloured. Nonetheless, the random-access technique still greatly outperformed forward rendering.

It is also interesting to note that the performance of random-access encoding and rendering combined almost perfectly matched traditional rendering of the text image, which means animated text can be rendered with equal efficiency using both techniques.

8   Conclusion and Future Work

We have presented a preprocessing and rendering technique for vector images which takes advantage of the parallel architecture of the GPU and allows fast random access rendering of animated vector images. We have shown that our approach roughly matches the memory requirements of a traditional bitmap image, outperforms the CPU in the preprocessing step and matches or in some cases significantly outperforms the traditional forward rendering technique.

Our pivot-point vector image representation performs slightly better and requires significantly less memory compared to the auxiliary-segment representation. It retains the traditional advantage of

scalability over bitmap images, while offering additional advantage in terms efficient texture mapping.

Due to time constraints, our implementation does not support all the features of a typical vector image. Moreover, there are areas where alternative approaches could provide further performance gains. Avenues for future work include:

1. Rendering of wide strokes by approximation with filled paths

2. Colouring shape interior based on a linear or radial gradient

3. Use of adaptive rather than fixed approximation of cubic segments with quadratic segments

4. Implementation of efficient ray intersection with cubic segments to avoid approximation entirely and reduce stream memory size

5. Use of heterogeneous data types and alignment of cell stream data structures in GPU memory for more efficient access

6. Generalisation of pivot-point representation to irregular spatial data structures, such as a kd-tree

8.1   Non-traditional Applications

Besides the traditional advantage of scalability, a localised vector image representation offers additional advantage in the form of efficient random-access which allows alternative non-traditional applications.

Figure 19 shows the tiger and text images used as textures and mapped onto the surface of a cylinder under perspective transformation. Such application was previously limited to bitmap textures and the artifacts introduced at larger levels of zoom were limiting the flexibility of use. Instead, vector textures could be used in many ways to enhance user experience in desktop applications as well as virtual worlds.

Vector-based glyphs and other user interface elements can retain sharpness when rendered on a slanted or curved surface at any scale. This allows for much greater flexibility and creativity in user interface design and facilitates development of 3-dimensional desktop interfaces, which can lead to general improvement in screen estate management.

In virtual worlds, bitmap textures suffer from artifacts when the viewer approaches the textured surface. In order to retain the image clarity, a sufficiently large bitmap has to be used to still read well at the closest distance it is expect to be observed from. This leads to suboptimal memory usage when a textured object is observed from afar. Traditionally, to work around this issue, multiple versions of the same image of various sizes would be used and loaded depending on the viewer's position. However, when a vector texture is used, a single version of the image needs to be loaded in memory to be able to render the textured object with maximum clarity regardless of the viewer's position.

Lorem ipsum dolor sit amet, consectetur adipisicing elit, sed do eiusmod tempor incididunt ut labore et dolore magna aliqua. Ut enim ad minim veniam, quis nostrud exercitation ullamco laboris nisi ut aliquip ex ea commodo consequat. Duis aute irure dolor in reprehenderit in voluptate velit esse cillum dolore eu fugiat nulla pariatur. Excepteur sint occaecat cupidatat non proident, sunt in culpa qui officia deserunt mollit anim id est laborum.

Lorem ipsum dolor sit amet, consectetur adipisicing elit, sed do eiusmod tempor incididunt ut labore et dolore magna aliqua. Ut enim ad minim veniam, quis nostrud exercitation ullamco laboris nisi ut aliquip ex ea commodo consequat. Duis aute irure dolor in reprehenderit in voluptate velit esse cillum dolore eu fugiat nulla pariatur. Excepteur sint occaecat cupidatat non proident, sunt in culpa qui officia deserunt mollit anim id est
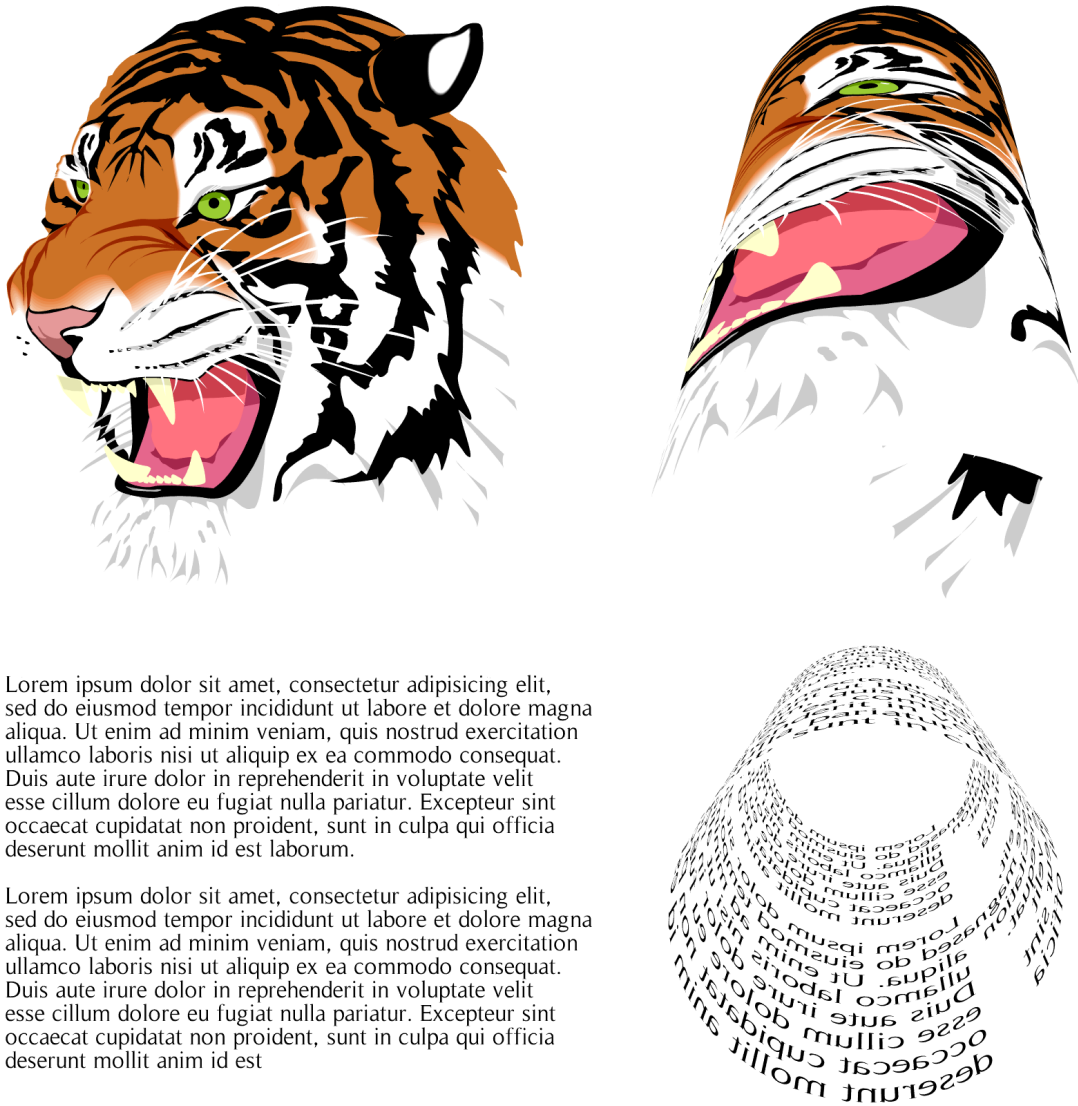
Figure 19: Tiger and text vector images used in our tests. On the left, the image rendered onto a flat surface. On the right, the image mapped onto a curved surface of a cylinder.

References

[BM99]   Wolfgang Boehm and Andreas Mller. On de casteljau's algorithm. *Computer Aided Geometric Design*, 16(7):587 – 605, 1999.

[Far02]   Gerald Farin. *Curves and surfaces for CAGD: a practical guide*. Morgan Kaufmann Publishers Inc., San Francisco, CA, USA, 5th edition, 2002.

[KSST06]   Yoshiyuki Kokojima, Kaoru Sugita, Takahiro Saito, and Takashi Takemoto. Resolution independent rendering of deformable vector objects using graphics hardware. In *SIGGRAPH '06: ACM SIGGRAPH 2006 Sketches*, page 118, New York, NY, USA, 2006. ACM.

[LB05]   Charles Loop and Jim Blinn. Resolution independent curve rendering using programmable graphics hardware. In *SIGGRAPH '05: ACM SIGGRAPH 2005 Papers*, pages 1000–1009, New York, NY, USA, 2005. ACM.

[NH08]   Diego Nehab and Hugues Hoppe. Random-access rendering of general vector graphics. In *SIGGRAPH Asia '08: ACM SIGGRAPH Asia 2008 papers*, pages 1–10, New York, NY, USA, 2008. ACM.